

DL_POLY Quantum 2.0: A modular general-purpose software for advanced path integral simulations

Cite as: J. Chem. Phys. 160, 132501 (2024); doi: 10.1063/5.0197822

Submitted: 14 January 2024 • Accepted: 12 March 2024 •

Published Online: 1 April 2024



View Online



Export Citation



CrossMark

Nathan London,¹ Dil K. Limbu,^{1,2} Mohammad R. Momeni,^{1,a)} and Farnaz A. Shakib^{2,b)}

AFFILIATIONS

¹ Division of Energy, Matter and Systems, School of Science and Engineering, University of Missouri—Kansas City, Kansas City, Missouri 64110, USA

² Department of Chemistry and Environmental Science, New Jersey Institute of Technology, Newark, New Jersey 07102, USA

^{a)}E-mail: mmomenitaheri@umkc.edu

^{b)}Author to whom correspondence should be addressed: shakib@njit.edu

ABSTRACT

DL_POLY Quantum 2.0, a vastly expanded software based on DL_POLY Classic 1.10, is a highly parallelized computational suite written in FORTRAN77 with a modular structure for incorporating nuclear quantum effects into large-scale/long-time molecular dynamics simulations. This is achieved by presenting users with a wide selection of state-of-the-art dynamics methods that utilize the isomorphism between a classical ring polymer and Feynman's path integral formalism of quantum mechanics. The flexible and user-friendly input/output handling system allows the control of methodology, integration schemes, and thermostating. DL_POLY Quantum is equipped with a module specifically assigned for calculating correlation functions and printing out the values for sought-after quantities, such as dipole moments and center-of-mass velocities, with packaged tools for calculating infrared absorption spectra and diffusion coefficients.

Published under an exclusive license by AIP Publishing. <https://doi.org/10.1063/5.0197822>

I. INTRODUCTION

Classical molecular dynamics (MD)^{1–4} has been a powerful tool in calculating macroscopic, i.e., experimentally observable, thermodynamic, and dynamic properties of a wide variety of physical, chemical, and biological systems.^{5–8} Invoking the Born–Oppenheimer approximation⁹ on the separation of electronic and nuclear motion and utilizing the laws of classical mechanics, MD presents an unparalleled time efficiency for long-time/large-scale simulations. On the downside, it neglects nuclear quantum effects (NQEs)¹⁰ associated with atomic motions. This can lead to incorrect scenarios when NQEs, such as tunneling and zero-point energy, are deterministic factors in the mechanism, rate, and efficiency of condensed-phase dynamics. In response, the well-known isomorphism^{11–14} between Feynman's path integral formulation of quantum mechanics¹⁵ and a classical ring polymer of n beads has been exploited extensively for calculating condensed-phase statistical and dynamical properties subject to NQEs.^{16–18} Rahman and Parrinello studied the properties of an electron solvated in molten

KCl by imparting fictitious kinetic energy in the discretized version of the path integral (PI) Hamiltonian, essentially formulating path integral molecular dynamics (PIMD) for investigating equilibrium properties.¹⁹ This was followed by the introduction of centroid molecular dynamics (CMD)^{20–22} and ring polymer molecular dynamics (RPMD)^{23–25} to make use of PI formulation in modeling the real-time dynamics in condensed phases.

Despite the exciting potentials and extensive successes of PI approaches, even in the case of non-adiabatic quantum dynamics,^{26–32} their approximate nature can lead to deviation from the correct physical behavior in the study of specific reaction regimes or calculating certain properties. A very well-known example is the intrinsic problems of CMD and RPMD in quantitative simulation of infrared absorption spectra.^{33,34} Nevertheless, inclusion of NQEs into MD simulations via classical trajectories with an extended phase space provides a computational efficiency that is not achievable with fully quantum mechanical approaches. As such, a number of distinct codes have been developed over the years for performing PI simulations. While many of these codes are exclusive to individual research

groups and only offer limited applications, considerable efforts were also made in bringing PI simulations to the mainstream by developing open-source and publicly available software packages. The most renowned i-PI,³⁵ a universal force engine interface written in Python, is a modular software that allows a range of PI simulations with a variety of user-controlled features. Contingent upon an interface with external software packages for the calculation of forces, i-PI also offers ways of reducing computation time using state-of-the-art ring polymer contraction^{36,37} and multiple time stepping.^{37,38} Recently, the MD simulation package LAMMPS³⁹ has also been equipped with PI simulations, though only offering two options of PIMD or CMD methods.

Here, adding to and expanding upon the existing repertoire, we introduce DL_POLY Quantum 2.0 as a highly modular and user-friendly computational platform for advanced PI simulations. It is the newest version of our DL_POLY Quantum 1.0,⁴⁰ which was a modified version of DL_POLY Classic 1.10,⁴¹ a highly parallelized software for classical MD simulations. DL_POLY Quantum 2.0 is a stand-alone software that offers a diverse range of PI simulations in a computationally efficient manner so that the users can test different flavors of path integrals for their systems of interest by invoking simple keywords in the input file and make a proper choice of the appropriate methodology. Written in FORTRAN, DL_POLY Quantum 2.0 is most suitable for high-performance computing and provides significant time efficiency. Furthermore, the modular architecture makes it accessible for future methodological implementations or interfacing with other existing packages. One of the notable features of DL_POLY Quantum 2.0 is the correlation module, which offers the capability to calculate velocity and dipole correlation functions. The module operates outside any integration method, allowing its use for any implemented real-time dynamics simulation. In the next sections, we present an overview of the PI formalism and the methods implemented in DL_POLY Quantum 2.0. We then discuss the features of our DL_POLY Quantum 2.0 code and its performance. We will complement these discussions with representative simulated test cases and relevant results and will wrap up with a discussion of future development plans for the software.

II. PATH INTEGRAL FORMALISM

As mentioned above, the main goal of DL_POLY Quantum is to offer a suite of many path integral based dynamics methods in a modular and extrapolatable suite that is easy to use. In this section, we outline and differentiate, wherever necessary, the theory of different path integral approaches implemented in DL_POLY Quantum 2.0.

A. Path integral molecular dynamics

The general Hamiltonian for a one-dimensional system of N particles is written as

$$\hat{H} = \sum_{i=1}^N \frac{\hat{p}_i^2}{2m_i} + \hat{V}(\mathbf{x}), \quad (1)$$

where $\mathbf{x} = \{x_1, \dots, x_N\}$ and $\mathbf{p} = \{p_1, \dots, p_N\}$ are position and momentum vectors, respectively, m_i is the mass of the i th particle, and $\hat{V}(\mathbf{x})$ is the potential energy operator of the system. The canonical partition function for this system is

$$Z = \text{Tr} [e^{-\beta \hat{H}}], \quad (2)$$

where $\beta = (k_B T)^{-1}$ is the reciprocal temperature. When subject to the Feynman path integral formulation⁴² and Trotter approximation,⁴³ the trace in Eq. (2) becomes a classical phase space integral,

$$Z_n \propto \int d^f \mathbf{x} \int d^f \mathbf{p} e^{-\beta H_n(\mathbf{x}, \mathbf{p})}, \quad (3)$$

where $f = Nn$ and n is the number of imaginary time slices, or “beads,” of the path integral. Z_n becomes equal to Z in the infinite bead limit. The PIMD Hamiltonian in Eq. (3) is defined as

$$H_n(\mathbf{x}, \mathbf{p}) = \sum_{i=1}^N \sum_{\alpha=1}^n \left[\frac{p_{i,\alpha}^2}{2m'_i} + \frac{1}{2} m_i \omega_n^2 (x_{i,\alpha} - x_{i,\alpha-1})^2 \right] + \frac{1}{n} \sum_{\alpha=1}^n V(x_{1,\alpha}, \dots, x_{N,\alpha}), \quad (4)$$

where $x_{i,\alpha}$ and $p_{i,\alpha}$ are the position and momentum of the α th bead of the i th particle, m'_i is the fictitious Parrinello–Rahman mass,¹⁹ and $\omega_n = \frac{\sqrt{n}}{\beta \hbar}$. The cyclic nature of the trace in Eq. (2) requires that $x_{i,0} = x_{i,n}$, creating a closed chain of ring polymer beads.

The PIMD method can be used to calculate quantum mechanical equilibrium properties from classical trajectories. Within the PI framework, the expectation value of an operator, \hat{A} , is

$$\langle A \rangle = \frac{1}{Z} \text{Tr} [e^{-\beta \hat{H}} \hat{A}] \approx \frac{1}{(2\pi\hbar)^f Z_n} \int d^f \mathbf{x} \int d^f \mathbf{p} e^{-\beta H_n(\mathbf{x}, \mathbf{p})} A_n(\mathbf{x}), \quad (5)$$

where

$$A_n(\mathbf{x}) = \frac{1}{n} \sum_{\alpha=1}^n A(x_{\alpha}) \quad (6)$$

is the bead-averaged value of the operator. These expectation values can be computed by time averaging the value of the operator over PIMD trajectories, as is commonly done in classical MD simulations. The equations of motion (EOMs) derived from the PIMD Hamiltonian are

$$\begin{aligned} \dot{p}_{i,\alpha} &= -m_i \omega_n^2 (2x_{i,\alpha} - x_{i,\alpha-1} - x_{i,\alpha+1}) + \frac{1}{n} \nabla_{x_{i,\alpha}} V(\mathbf{x}) \\ \dot{x}_{i,\alpha} &= \frac{p_{i,\alpha}}{m'_i}. \end{aligned} \quad (7)$$

To ensure that the configurations sampled during the trajectories are part of the correct Boltzmann distribution, PIMD simulations are performed in the canonical ensemble by coupling the dynamics to a thermostat. A number of different thermostats are implemented in DL_POLY Quantum 2.0, including conventional MD thermostats and PI specific thermostats, which will be thoroughly explained in the Sec. III.

Straightforward implementation of the PIMD Hamiltonian and its EOMs in Cartesian coordinates is complicated by the harmonic coupling between neighboring beads. Most implementations of the method transform the Hamiltonian into a different coordinate system, which diagonalizes the couplings. DL_POLY Quantum offers two different implementations of PIMD using staging variables and

normal mode coordinates. The detailed explanations of these two transformations are presented in [Appendix A](#). Here, it is suffice to mention that the PIMD Hamiltonian in normal modes is

$$H_{\text{NM}} = \sum_{i=1}^N \sum_{k=0}^{n-1} \left[\frac{\pi_{i,k}^2}{2m_i} + \frac{1}{2} m_i \omega_k^2 q_{i,k}^2 \right] + \frac{1}{n} \sum_{\alpha=1}^n V(x_{1,\alpha}(\mathbf{q}), \dots, x_{N,\alpha}(\mathbf{q})), \quad (8)$$

where $\omega_k = 2\omega_n \sin(k\pi/n)$ are normal mode frequencies and $q_{i,k}$ and $\pi_{i,k}$ are the positions and momenta, respectively, for the k th normal mode of the i th atom.

B. Ring polymer molecular dynamics

Introduced by Craig and Manolopoulos,^{23–25} RPMD is an approximate quantum dynamics method that utilizes the PIMD Hamiltonian to perform real-time dynamics. While there is no rigorous derivation of RPMD from real-time quantum dynamics, numerical simulations have demonstrated the effectiveness of the method.^{24,44–46}

The RPMD Hamiltonian differs slightly from the PIMD Hamiltonian of Eq. (4), as it is taken to be

$$H_n(\mathbf{x}, \mathbf{p}) = \sum_{i=1}^N \sum_{\alpha=1}^n \left[\frac{p_{i,\alpha}^2}{2m_n^{(i)}} + \frac{1}{2} m_n^{(i)} \omega_n^2 (x_{i,\alpha} - x_{i,\alpha-1})^2 \right] + \frac{1}{n} \sum_{\alpha=1}^n V(x_{1,\alpha}, \dots, x_{N,\alpha}), \quad (9)$$

with $m_n^{(i)} = \frac{m_i}{n}$ and $\omega_n = \frac{n}{\beta\hbar}$. Note that the fictitious mass in the kinetic energy term must be equal to the physical mass, with the additional factor of $\frac{1}{n}$ multiplying the physical mass coming from sampling the initial momenta at the physical temperature, β , instead of a higher temperature, $\beta_n = \frac{\beta}{n}$, as is often done in RPMD simulations.

RPMD simulations can be performed utilizing the same normal mode integration scheme as with PIMD (see [Appendix A 2](#)) but without coupling the dynamics to any thermostating method.

C. Partially adiabatic centroid molecular dynamics

In CMD, the particle is evolved in real time under the effective mean-field potential of an imaginary time ring polymer with its centroid constrained at the position of the particle.^{20–22} Adiabatic implementations of CMD were created to allow for the mean-field potential to be calculated “on-the-fly” during the dynamics.²⁰ This is achieved by using the physical mass of the particle as the centroid mass, scaling down the mass of the non-centroid internal modes of the Ring Polymer (RP), and attaching the internal modes to a thermostat so that they sample the equilibrium distribution, while being constrained to the position of the slower moving centroid.²⁰ Full adiabatic separation requires a very small mass for the internal modes and thus a very small integration time step. This led to the development of the partially adiabatic centroid molecular dynamics (PA-CMD) method, in which the mass scaling is not as extreme, allowing for a larger time step while still providing accurate dynamics.⁴⁷

The PA-CMD effective Hamiltonian in terms of the free ring polymer normal modes is⁴⁷

$$H_{\text{PA-CMD}}^0 = \sum_{i=1}^N \sum_{k=0}^{n-1} \left[\frac{\pi_{i,k}^2}{2\sigma_k^2 m_n^{(i)}} + \frac{1}{2} m_n^{(i)} \omega_k^2 q_{i,k}^2 \right], \quad (10)$$

where σ_k is a scaling factor defined as

$$\sigma_k = \begin{cases} 1, & k = 0, \\ \omega_k/\Omega, & k \neq 0, \end{cases} \quad (11)$$

and the normal mode masses and frequencies are the same as that for RPMD. The choice of Ω , which is related to the adiabaticity parameter of the original PA-CMD, determines how adiabatically separated the centroid is from the other internal modes. One such choice is³³

$$\Omega = \frac{n^{n/(n-1)}}{\beta\hbar}. \quad (12)$$

This specific choice pushes the frequencies of the internal modes to be outside the spectral range of interest to avoid the spurious frequencies of the RPMD spectra, while allowing for the largest integration time step.

To ensure the necessary canonical sampling of the internal modes to generate the centroid potential of the mean force needed to evolve the centroid, the internal modes are coupled to a thermostat. In DL_Poly Quantum 2.0, PA-CMD is implemented with the massive Nose-Hoover Chain (NHC) thermostat. When calculating the correlation functions, only the centroid contributes to the operators, resulting in

$$A_n(\mathbf{x}) = A_n(\tilde{x}), \quad (13)$$

where $\tilde{x} = \frac{1}{n} \sum_{\alpha=1}^n x_{\alpha}$ is the RP centroid.

III. PROGRAM OVERVIEW AND FEATURES

DL_Poly Quantum 2.0 is designed as a generalized, path integral extension to the DL_Poly Classic 1.10 program, utilizing both the original code and its overall architecture. The additions to the program keep its modular nature intact, allowing for a straightforward path for future additional functionality. DL_Poly Quantum 2.0 offers a variety of PI dynamics methods, expanding on the PIMD module from DL_Poly Classic 1.10. The required input files (i.e., CONTROL, FIELD, and CONFIG files) and the basic output files (i.e., OUTPUT, STATIS, and HISTORY files) are unchanged. Furthermore, the program still allows utilizing the originally implemented features in DL_Poly Quantum 1.0. To highlight the structure of the code and the changes made in the current version, [Fig. 1](#) presents a flowchart for a PI simulation, including a correlation function calculation. In particular, it shows the interactions between our new, or heavily modified modules, and the existing modules in DL_Poly Classic. More details on the implemented features in DL_Poly Quantum suite are listed in the following.

A. DL_Poly Quantum suite: Features of version 1.0

- The flexible four-site q-TIP4P/F quantum water potential⁴⁸ is implemented for both classical and path integral simulations. This is a fixed-point charge model for liquid water

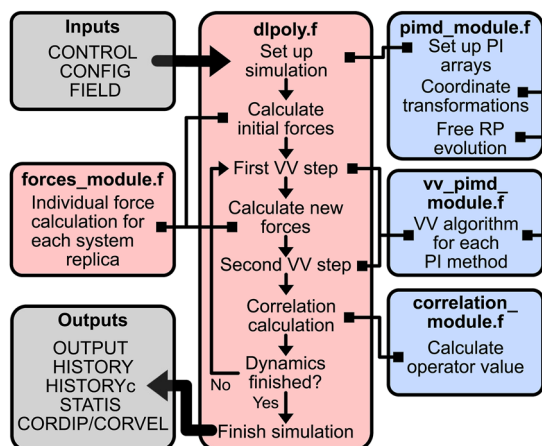


FIG. 1. Flowchart of the major modules used for a PI simulation with correlation calculation in DL_POLY Quantum 2.0. The gray boxes indicate the input and output files. The red boxes indicate modules from DL_POLY Classic 1.10 with minor or no changes to them. The blue boxes indicate the modules that have either been added or heavily modified. Here, VV stands for the velocity Verlet algorithm.

in which the O–H stretches are described by Morse-type functions. A new module called *water_module.f* is added to the suite, which includes several subroutines needed to simulate water dynamics. The input files should be changed accordingly; the CONTROL file should contain the keyword **QTIP4PF**. In the CONFIG file, each water molecule should include the M-site as the 4th atom with zero mass.

- Nosé–Hoover chain (NHC) thermostat is implemented for classical MD simulations in the canonical NVT ensemble based on the Suzuki–Yoshida scheme.^{49,50} The NH thermostat was already available in DL_POLY Classic for creating an NVT ensemble. However, NH equations fail when the system obeys more than one conservation law.⁴ To counterbalance this, more phase space dimensions must be introduced, which can be accomplished by introducing a chain of interconnected NH thermostats, resulting in the gold-standard NHC thermostat. In DL_POLY Quantum suite, this is achieved by adding a subroutine called **NVTVV_NHC** in *vv_motion_module.f*, which calls for the subroutine **NHC_part** in *integrator_module.f*. The classical MD simulation is activated by the keywords **NVT** and **NHC** in the CONTROL file.
- The NHC thermostat/barostat for isothermal–isobaric NPT ensemble through the Martyna–Tobias–Klein (MTK) algorithm^{51,52} is implemented for classical MD simulations. The experiments are more commonly performed at conditions of constant pressure rather than constant volume, requiring simulations to be performed in the NPT ensemble. The canonical ensemble from our NVT NHC implementation forms the basis for the NPT simulations. To maintain a fixed internal pressure, the system's volume is allowed to fluctuate isotropically. This implementation is achieved through adding the subroutine **NPTVV_NHC** in *vv_motion_module.f*, which calls for two subroutines,

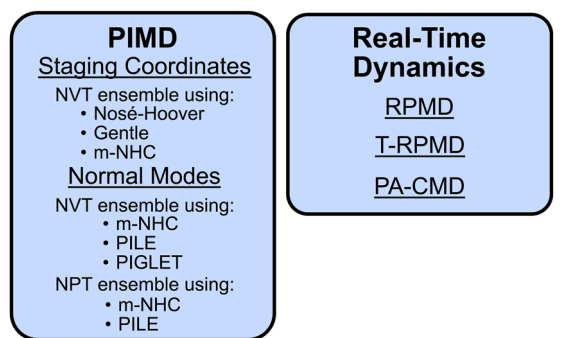


FIG. 2. Summary of the path integral methods available in DL_POLY Quantum 2.0.

NHC_part and NHC_baro, in *integrator_module.f*. The classical MD simulation is activated by the keywords **NPT** and **NHC** in the CONTROL file.

B. DL_POLY Quantum suite: Features of version 2.0

A summary of the different PI methods available in DL_POLY Quantum 2.0 is shown in Fig. 2. In particular, it emphasizes which ensembles and thermostats can be used for PIMD simulations. More details of the different features implemented in DL_POLY Quantum 2.0 are summarized below.

- PIMD simulations in normal mode coordinates are implemented in DL_POLY Quantum 2.0. This complements PIMD in staging coordinates,⁵³ which was already available in DL_POLY Classic 1.10. PIMD in staging coordinates can be performed with a single NH thermostat,⁵³ a “gentle” thermostat,⁵⁴ or the massive NHC (*m*-NHC) thermostat.^{53,55} These options can be selected with the keywords **PIMD NVT**, **PIMD GTH**, and **PIMD NHC** in the CONTROL file, respectively. The normal mode implementation is performed within the already existing *vv_pimd_module.f*; the additional subroutine **PIMD_NVT_NHC_NM**. PIMD simulations using normal modes with an *m*-NHC thermostat are selected using the keywords **PIMD NM** in the CONTROL file. Note that PIMD simulations with the additional PI specific thermostats and the real-time methods outlined below, are all performed in normal modes.
- Path integral Langevin equation (PILE) thermostat:⁵⁶ in PIMD simulations, quantum nuclei are represented as a collection of fictitious particles, and the system's behavior is explored by sampling over all possible configurations of these particles. Traditional thermostats used in classical simulations may not suffice in the context of PIMD, where quantum fluctuations are prominent. PILE is a specialized stochastic thermostat for controlling the temperature of PI simulations, which exploits an analytic knowledge of the free PI normal mode frequencies. The subroutine **PIMD_NVT_PILE_NM** was added in *vv_pimd_module.f*. The PILE thermostat can be selected using the keywords **PIMD PILE** in the CONTROL file.

- Path integral generalized Langevin equation thermostat (PIGET) is implemented in the canonical NVT ensemble.⁵⁷ PIGET is a stochastic thermostat for accurately modeling the thermal fluctuations within the quantum systems in PI simulations. A practical implication of PI simulations with the PIGET thermostat is that convergence can be reached using ring polymers with fewer number of beads compared to the reference PIMD simulations with *m*-NHC or PILE thermostats. A new module, *pimd_piglet_module.f*, has been introduced to incorporate the PIGET thermostat into PIMD simulations, and the subroutine PIMD_NVT_PIGET was added in *vv_pimd_module.f*. The PIGET thermostat can be selected using the keywords **PIMD PIGET** in the CONTROL file.
- Simulations at fixed pressure and temperature, i.e., NPT ensemble, are also available for PI simulations with an *m*-NHC thermostat/barostat and PILE with isotropic cell fluctuations. Subroutine PIMD_NPT_NHC_NM and PIMD_NPT_PILE_NM were added in the module *vv_pimd_module.f*, which can be invoked by including **PIMD NPT NHC** and **PIMD NPT PILE** in the CONTROL file, respectively.
- RPMD simulations can be performed utilizing the same normal mode integration scheme as with our newly implemented normal mode PIMD but without coupling the dynamics to a thermostat. This is accomplished using the subroutine PIMD_NVE in *vv_pimd_module.f*. RPMD simulations are invoked with the keywords **PIMD NVE** in the CONTROL file.
- Thermostatted (T)-RPMD⁵⁸ couples the internal modes of the ring polymer to a thermostat without altering their masses. This removes the spurious oscillations of the internal modes of the ring polymer from standard RPMD. During the dynamics, the internal modes are coupled to the PILE thermostat, while the centroid is not thermostatted. T-RPMD is implemented using the TRPMD subroutine in *vv_pimd_module.f*. It is invoked by including the keywords **PIMD TRPMD** in the CONTROL file.
- PA-CMD simulations are performed using the PACMD subroutine in *vv_pimd_module.f* and can be chosen with the keywords **PIMD PACMD** in the CONTROL file.
- The final notable feature is a new module, *correlation_module.f*, which offers the capability to calculate velocity and dipole correlation functions from both classical and PI dynamics simulations. The module operates outside any integration method, allowing its use for any implemented real-time dynamics simulations. Real-time correlation functions are directly calculated by specifying the keywords **CORRELATION DIPOLE** and **CORRELATION VELOCITY** in the CONTROL file for dipole moment and velocity, respectively. The correlation functions calculated in DL_POLY Quantum 2.0 are all autocorrelation functions of the specified operator for a single type of molecule. For heterogeneous systems, the desired molecule is chosen by adding the molecule type number after the keywords to invoke the correlation function calculation in the CONTROL file (e.g., **CORRELATION DIPOLE mol = 2** for the second molecule type). The molecule type number is

specified by the order of the molecules defined in the FIELD file.

- It should be noted that a correction has been introduced to rectify inconsistent volume fluctuations in multi-core NPT simulations in the original DL_POLY Classic 1.10. The observed variations in volume fluctuations across different cores were attributed to inconsistent electrostatic virial values, resulting from 1 to 4 interactions in the subroutine DIHFRC of module *dihedral_module.f*. This inconsistency arose due to the absence of initialization for certain parameters. The correction aims to ensure proper initialization of these parameters, thereby resolving the issue and ensuring consistent total virial across all cores in parallel simulations.

IV. CODE PERFORMANCE AND EFFICIENCY

PI simulations have an inherent increased computational cost compared to classical MD simulations as the system is essentially *n* times larger than the equivalent classical system. Thus, it is important for any PI-based dynamics program to be sufficiently efficient to reduce the overall computational cost and be properly parallelized to reduce the wall-time of simulations.

Parallelization in DL_POLY Quantum 2.0 is adopted from DL_POLY Classic 1.10 and takes the form of the data replication strategy.^{59,60} In this scheme, important quantities, such as position, velocity, and force arrays, are replicated across all cores. This method ensures that at the start of a given parallel calculation, all cores

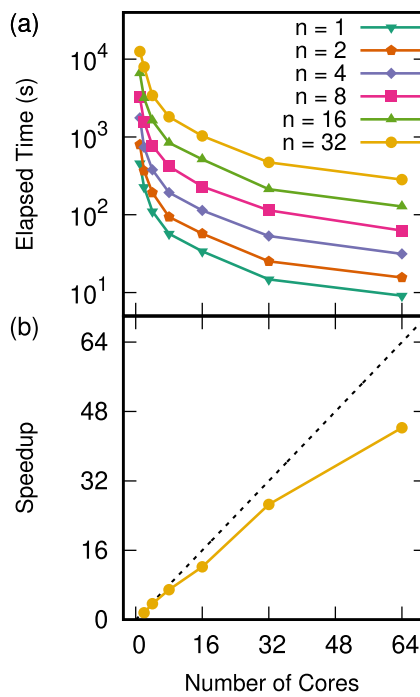


FIG. 3. (a) Calculated wall-times for 1000 time steps of PIMD simulations for 1728 q-TIP4P/F water molecules using the PILE thermostat with various numbers of beads *n* and computational cores averaged over three independent runs. (b) Calculated relative speedup of simulations for *n* = 32 beads, with the dashed line representing a linear speedup.

have the current system information and the calculation can be evenly distributed across the cores, regardless of the configuration of the simulation cell. After the calculation, the new values are then updated across all cores. While this scheme can lead to higher memory usage and communication overhead compared to other MD parallelization strategies, its ability to distribute work more evenly among cores has proven it to be useful for a range of applications.⁶⁰ The division of calculations across cores does not change with the number of beads for PI simulations as the parallelization is based on a single replica of the system. For calculations such as updating the positions and velocities, a loop over the beads for a given atom is performed. Force calculations are performed as a loop over system replicas where all beads have the same index. This accounts for the fact that only beads of different ring polymers with the same index interact and restricts all force calculations to only include the N atoms of the system.

To demonstrate the performance of DL_Poly Quantum 2.0, a series of PIMD NVT simulations of bulk water, described using the q-TIP4P/F water model, are performed for a varied number of beads utilizing a varied number of cores. The unit cell is comprised of 1728 water molecules with a density of 0.997 g/cm^{-3} . The temperature is kept constant at 300 K using the PILE thermostat. All performance benchmarking simulations presented here were performed on the SSE Machine Learning Cluster at the University of Missouri, Kansas City, using AMD EPYC 7H12 processors. All simulations are evolved for 1000 steps with a time step of 0.2 fs and with a thermostat time constant of 0.05 ps.

The wall-time of these simulations are presented in Fig. 3(a). For all bead numbers, there is a significant reduction in the computation time for a small increase in the number of cores used.

Diminishing time reduction is seen for larger number of cores as the communication overhead increases from the data replication parallelization. The relative speedup when using multiple cores is found by comparing the wall-time of that simulation to that of the single-core simulation. The speedup for the simulations with 32 beads is shown in Fig. 3(b). As expected from the calculated wall-times, the relative speedup for a small number of cores is near linear but drops off for increased number of cores. Overall, DL_Poly Quantum 2.0 displays successful parallelization for large systems.

V. EXAMPLES OF NEW FEATURES

In order to demonstrate the broad applicability range of the DL_Poly Quantum suite, a few example cases are discussed in this section.

A. Incorporating NQEs into large-scale simulations: HKUST-1 metal-organic framework

Metal-organic frameworks (MOFs) are a promising class of nanoporous hybrid organic/inorganic materials with a wide spectrum of applications in energy storage,^{61–63} catalysis,^{64–67} electronics,^{68–72} and water harvesting and purification.^{73–75} Considering the prohibitively expensive cost of “on-the-fly” *ab initio* molecular dynamics (AIMD), classical MD simulations using analytical force fields (FF) have been a leading approach in simulating both dry and guest adsorbed MOFs. Nevertheless, both AIMD and MD simulations suffer from neglecting NQEs. Here, we illustrate how the inclusion of NQEs changes the structural properties of the extended materials by comparing the MD and PIMD simulations

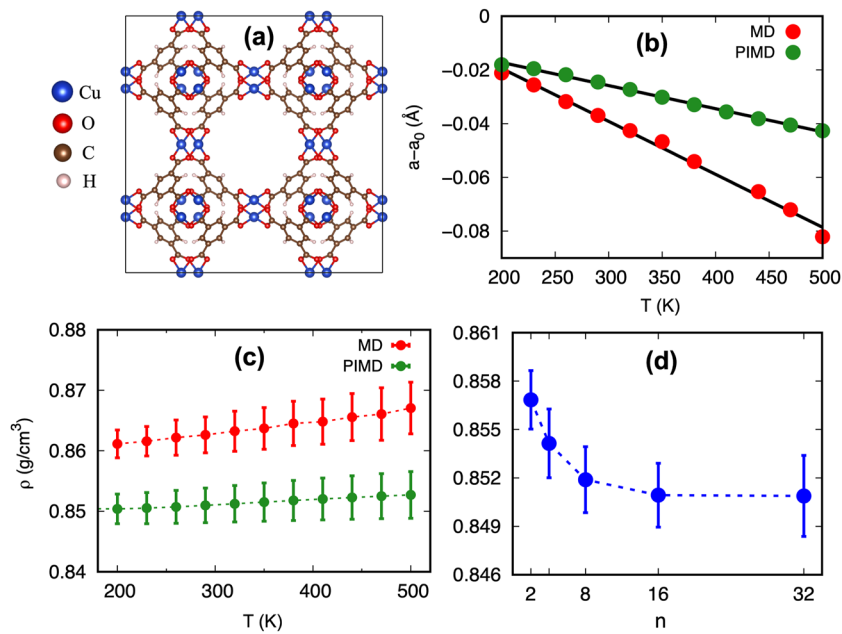


FIG. 4. (a) The cubic periodic unit cell of HKUST-1 containing 624 atoms and a cell length of 26.303 Å. (b) The calculated cell vector changes and (c) density as a function of temperature (T) using 1 ns MD (1 bead) and PIMD (32 beads) simulations. (d) The convergence of the calculated density of HKUST-1 at 200 K with respect to the number of beads in PIMD simulations.

of the archetypal HKUST-1 as a representative of the MOF family [Fig. 4(a)]. Since conventional FFs lack the parameters related to transition metals, several classes of FFs have been introduced for MOFs, including, but not limited to, universal force field for MOFs (UFF4MOFs),⁷⁶ MOF-FF,⁷⁷ Bristow-Tiana-Walsh (BTW) FF,⁷⁸ and *ab initio* parameterized FFs.^{79,80} For the simulations presented here, we make use of a modified BTW FF, where, for numerical stability, we replaced the original Buckingham potential for non-bonded interactions with a Lennard-Jones (LJ) potential. The details of the derivation of this BTW-LJ FF are provided in Appendix C.

Figure 4(b) shows the change in the unit cell vector of a $1 \times 1 \times 1$ unit cell of HKUST-1, comprised of 624 atoms, after 1 ns MD and PIMD simulations over a range of temperatures from 200 to 500 K. The temperature is kept constant using an NHC thermostat in MD and a PILE thermostat in PIMD simulations, as implemented in DL_POLY Quantum 2.0. In PIMD simulations, all atoms are represented by ring polymers composed of 32 beads. This information is used to calculate the linear expansion coefficient, $\alpha = \left(\frac{1}{a_0} \right) \left(\frac{\partial a}{\partial T} \right)_p$, where a is the unit cell vector length and a_0 is the reference unit cell vector of 26.303 Å length. Simulated values of $\alpha = -7.4 \times 10^{-6}$ and $-3.2 \times 10^{-6} \text{ K}^{-1}$ were obtained for MD and PIMD simulations, respectively, compared to the experimental value⁸¹ of $\alpha = -4.1 \times 10^{-6} \text{ K}^{-1}$. While both the results are consistent with the observed negative thermal expansion in MOFs, PIMD simulations provide a more accurate quantity due to the inclusion of NQEs in simulations. Figure 4(c) shows the linear increase in the density of HKUST-1 with temperature, attributed to the negative thermal expansion, where MD simulations overestimate this behavior. Figure 4(d) illustrates the convergence of the PIMD simulations for calculating the density of HKUST-1 at the lowest considered

temperature of 200 K. Notably, the results indicate that employing 16 beads is adequate for achieving a sufficiently converged outcome. All the presented results are based on averaging the final 800 ps of the simulation after the first 200 ps equilibration in a single 1 ns run. The average and the standard deviation are computed from these final 800 ps run data, and the error bars are shown based on the calculated standard deviation.

B. Utilization of path integral generalized Langevin equation thermostat

The path integral generalized Langevin equation thermostat (PIGET) is a powerful approach for improving computational efficiency in large scale simulations. This thermostat achieves efficiency gains by reducing the required number of beads for convergence of the results.⁸² Its effectiveness lies in exploiting the equivalence between non-Markovian dynamics in the generalized Langevin equation (GLE) framework and Markovian dynamics in a higher-dimensional space (p, s) , where n_s auxiliary momenta $s = \{s_i\}$ are introduced. These auxiliary momenta exhibit linear couplings with both the physical momentum and one another, resulting in a succinct representation of the stochastic differential equation. This approach significantly contributes to the streamlined optimization of simulations. More details about PIMD simulations using the PIGLET thermostat are presented in Appendix B.

In Fig. 5, we show our PIMD calculated radial distribution functions (RDFs) for 216 q-TIP4P/F bulk water at 298 K using the PIGLET thermostat with a different number of beads compared to the reference PIMD simulations with *m*-NHC thermostat and 32 beads. Similar to the original report by Ceriotti *et al.*,⁵⁷ performed using the same water potential model, our results show that

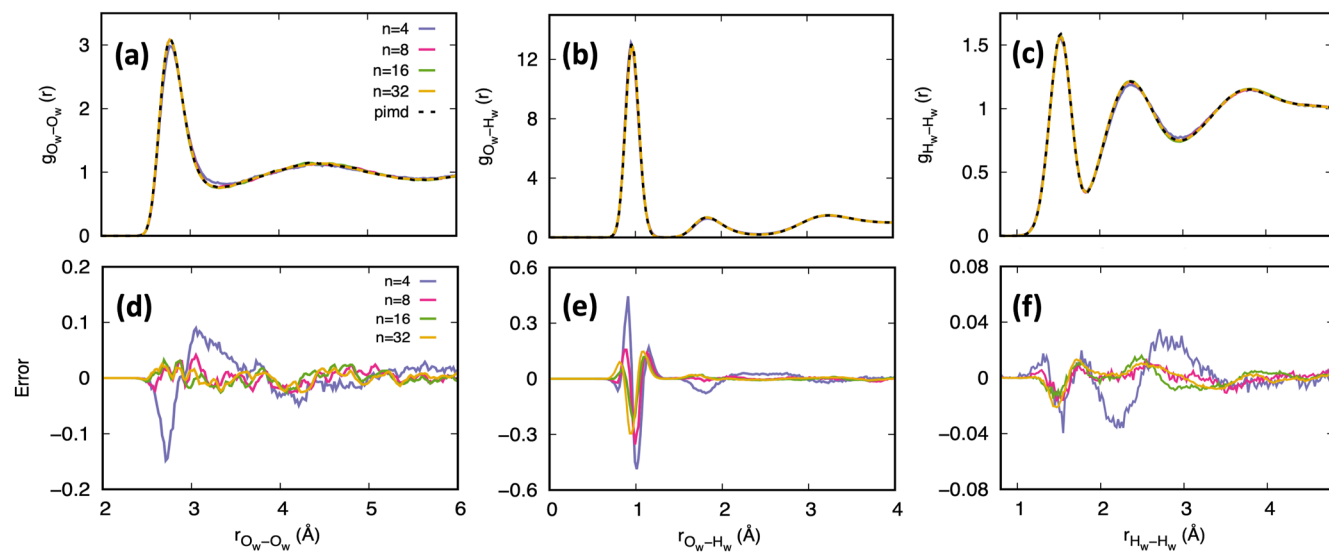


FIG. 5. (a)–(c) Calculated RDFs for 216 q-TIP4P/F bulk water at 298 K and in a cubic box with a side length of 18.64 Å utilizing periodic boundary conditions. Here, different RDFs obtained using the PIGLET thermostat with different number of beads are compared to the reference PIMD simulations using the *m*-NHC thermostat and 32 beads. (d)–(f) Corresponding errors.

PIGLET simulations with eight beads have already reached convergence compared to the reference PIMD simulations with the *m*-NHC thermostat.

VI. REAL-TIME DYNAMICS

The standard quantum mechanical correlation function between operators \hat{A} and \hat{B} is

$$C_{AB}(t) = \frac{1}{Z} \text{Tr} \left[e^{-\beta \hat{H}} \hat{A} e^{i \hat{H} t / \hbar} \hat{B} e^{-i \hat{H} t / \hbar} \right]. \quad (14)$$

This form of the correlation function does not have the same features as classical correlation functions. When looking to compare the two directly, it is preferable to use the Kubo-transformed correlation function instead, which has the following form:

$$\tilde{C}_{AB}(t) = \frac{1}{\beta Z} \int_0^{\beta} d\lambda \text{Tr} \left[e^{-(\beta-\lambda)\hat{H}} \hat{A} e^{-\lambda \hat{H}} e^{i \hat{H} t / \hbar} \hat{B} e^{-i \hat{H} t / \hbar} \right]. \quad (15)$$

The Kubo-transformed correlation function can be approximated in the path integral framework as²³

$$\tilde{C}_{AB}(t) \approx \frac{1}{(2\pi\hbar)^n Z_n} \int d\mathbf{p} \int d\mathbf{x} e^{-\beta_n H_n(\mathbf{p}, \mathbf{x})} A_n(\mathbf{x}) B_n(\mathbf{x}_t), \quad (16)$$

where \mathbf{x}_t is the configuration of the system at time t along a trajectory whose initial conditions are determined by the phase space integral. The zero-time value of Eq. (16) is just an integral in an extended

phase space and would give the same value as Eq. (15) in the limit of infinite number of beads.

DL_POLY Quantum is able to produce the necessary quantities to calculate two different correlation functions, velocity, and molecular dipole autocorrelation functions through a newly added correlation module. The program outputs the value of the operator for all molecules of a single type as a function of time that can be post-processed to calculate the correlation function and related quantities. The velocity autocorrelation function is used to obtain the diffusion coefficient, defined as

$$D = \frac{1}{3} \int_0^{\infty} dt \tilde{C}_{vv}(t). \quad (17)$$

For a molecule containing L atoms, the bead-averaged, center-of-mass velocity output is

$$v_i(t) = \frac{1}{nm_{\text{mol}}} \sum_{j \in i}^L \sum_{\alpha=1}^n p_{j,\alpha}(t), \quad (18)$$

where m_{mol} is the total mass of the molecule. The dipole autocorrelation function is used to calculate the IR spectrum. The IR signal is given by

$$n(\omega) \alpha(\omega) = \frac{\pi \beta \omega^2}{3cV\varepsilon_0} \tilde{I}(\omega), \quad (19)$$

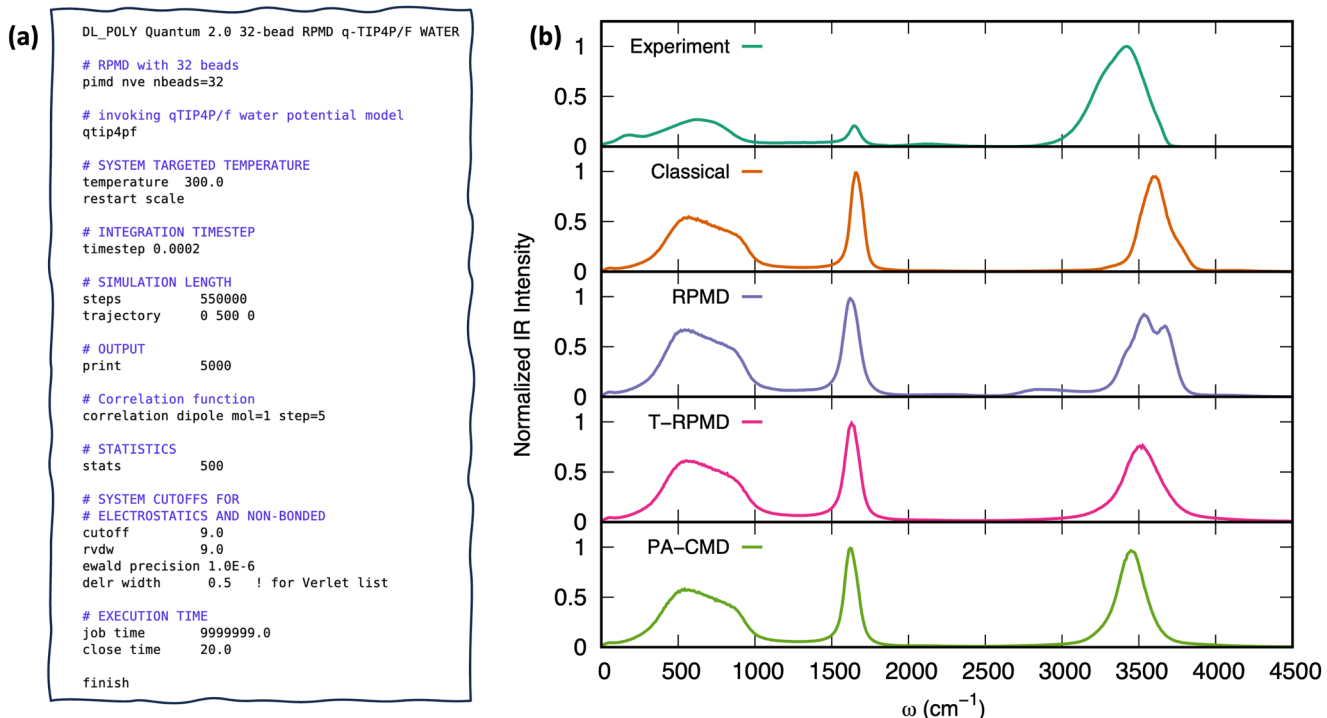


FIG. 6. (a) Example CONTROL file for RPMD simulation q-TIP4P/F water with dipole moment calculation. (b) Calculated IR spectra of liquid bulk water at 300 K. Using different PI flavors with 32 beads compared to the experimental spectrum from Ref. 83. See the text for more details.

where $\tilde{I}(\omega)$ is the Fourier transform of the dipole autocorrelation function,

$$\tilde{I}(\omega) = \frac{1}{2\pi} \int_{-\infty}^{\infty} dt e^{-i\omega t} \tilde{C}_{\mu\mu}(t). \quad (20)$$

The molecular dipole for a molecule with L atoms is calculated as

$$\mu_i(t) = \frac{1}{n} \sum_{j \in i}^L \sum_{\alpha=1}^n e_j(q_{j,\alpha})(t) - q_{\text{COM}}^{(i)}(t), \quad (21)$$

where e_j is the charge of the j th atom and $q_{\text{COM}}^{(i)}$ is the center-of-mass position of the molecule.

Following the approaches outlined above, Fig. 6 illustrates the IR spectra of liquid bulk water at 300 K using different PI methods, each with 32 beads. The spectra are obtained from simulations of 216 q-TIP4P/F water molecules in a cubic box with side lengths of 18.64 Å to achieve a density of 0.997 g/cm³. For all PI methods, the boxes are equilibrated for 20 ps using PIMD simulations evolved with a time step of 0.2 fs and thermostatted with an *m*-NHC thermostat with a chain length of 3 and a time constant of 0.05 ps. After equilibration, an additional 25 ps of PIMD simulations are run to generate the initial configurations for the real-time dynamics, which are taken every 1 ps.

The real-time dynamics for all PI methods are evolved with a time step of 0.2 fs. For PA-CMD, the internal modes are thermostatted at 300 K using an *m*-NHC thermostat with a chain length of 3 and a time constant of 0.05 ps. All trajectories are run for 110 ps, with the final 100 ps being used to calculate the spectra, which are averaged over 25 trajectories. The dipole moment operators are calculated every 5 time steps to ensure a sufficiently fine frequency grid when taking Fourier transform to produce the spectra. The spectrum for classical dynamics is calculated using the same method as just described but with a single-bead ring polymer.

Apart from the methods explained before, Fig. 6 also shows the results of thermostatted RPMD³⁸ (T-RPMD). It can be considered as an intermediate method between RPMD and CMD, which couples the internal modes of the RP to a thermostat without altering their masses. This helps remove the spurious frequencies from standard RPMD without the curvature problem of CMD. The T-RPMD Hamiltonian is the same as that for standard RPMD, where the internal modes are coupled to the PILE thermostat, while the centroid is not thermostatted.

In comparison between the experimental spectrum from Ref. 83 and the one obtained from classical MD simulations, one can see that due to neglecting NQEs, the latter is blue-shifted in the intramolecular O–H stretching and, to a lesser extent, bending regions. As such, the hydrogen bonding (HB) strength of liquid bulk water is underestimated by classical simulations. On the other hand, the RPMD spectrum is not reliable due to the contamination of the O–H stretches by the internal vibrational modes of the ring polymer,³³ while T-RPMD does remedy these artifacts by thermostating them. Finally, for the PA-CMD method, these modes are shifted beyond the spectral range of interest, providing the best estimate for the IR spectrum of liquid bulk water at 300 K compared to the experiment. In addition, in agreement with the literature,³³ our calculated spectra for liquid water at 300 K show that NQEs are less critical for the low-frequency librational bands. Overall, our calculated classical

and path integral IR spectra of the q-TIP4P/F liquid bulk water at 300 K agree with that of Manolopoulos and co-workers.³³ We have greatly simplified the process of generating these spectra using both classical and quantum PI simulations in DL_POLY Quantum 2.0. The source code is modified to calculate and write out the needed dipole operator values, and user-friendly post-analysis scripts are provided as part of the source code for performing the necessary analyses and creation of the final spectra.

VII. FUTURE DEVELOPMENTS

DL_POLY Quantum 2.0 improves upon version 1.0 through the introduction of several PI methods, as well as the ability to easily calculate operators for correlation functions, but there are many desirable features that are not included. To promote our plan to continue support and development for DL_POLY Quantum, we discuss here several features that we consider important enough to be implemented.

While we have demonstrated the performance of DL_POLY Quantum 2.0 in terms of its parallelization, besides PIGLET, we have not yet implemented any methods focused on specifically reducing the cost of PI simulations. A first step toward this effort is to ensure that the multiple time stepping algorithm, which was present in the original DL_POLY Classic, works for PI simulations as well. Additionally, implementing a ring polymer contraction scheme, which functions like multiple time stepping, but for the imaginary time slices of the ring polymer, would also reduce the cost of PI simulations.

To additionally increase the performance of our software, we will create a version of the software with graphical processing unit (GPU) support. GPU computing has proven to be successful in quantum chemistry calculations.^{84–86} A GPU-accelerated DL_POLY Quantum would look to push the expensive force calculations to the GPU, taking advantage of the extreme parallelization and minimal communication overhead of the GPU. The main control of the program and less demanding tasks, such as atom propagation, will remain with the CPUs. Adding GPU-acceleration would allow for DL_POLY Quantum to become an even more efficient software for performing large-scale PI simulations.

Finally, beyond increasing the efficiency of the code, we would like to expand its functionality. Of particular note is to introduce a new module to allow users to perform simulations utilizing machine learned potentials (MLPs). This would allow users to study complex systems for which there are no accurate analytical force fields and “on-the-fly” AIMD simulations are prohibitively expensive.

VIII. CONCLUSIONS

Here, we have introduced the software package DL_POLY Quantum 2.0, an updated version of DL_POLY Quantum 1.0, as a modular and user-friendly computational program for performing a wide variety of PI-based simulations. We have introduced new features and methods included in this new version of the software, including additional thermostats for PIMD simulations and several real-time dynamics methods. We also demonstrated its performance on different test systems, including bulk liquid water and

the HKUST-1 MOF system. Future versions of the software look to increase its efficiency and functionality.

ACKNOWLEDGMENTS

This research was partially supported by the National Science Foundation (Grant Nos. CBET-2302617 to F.A.S. and CBET-2302618 to M.R.M.) and the U.S. Department of Energy Office of Science, Basic Energy Sciences Program (Grant No. DE-SC0024512 to M.R.M.). This work used resources from Bridges-2 at Pittsburgh Supercomputing Center through Allocation Nos. CHE200007, CHE200008, and PHY230099 from the Advanced Cyberinfrastructure Coordination Ecosystem: Services & Support (ACCESS) program,⁸⁷ which is supported by National Science Foundation Grant Nos. 2138259, 2138286, 2138307, 2137603, and 2138296. Technical support and computing resources provided by the HPC centers at NJIT and UMKC is also gratefully acknowledged.

AUTHOR DECLARATIONS

Conflict of Interest

The authors have no conflicts to disclose.

Author Contributions

Nathan London: Software (equal); Writing – original draft (equal); Writing – review & editing (equal). **Dil K. Limbu:** Software (equal); Writing – original draft (equal); Writing – review & editing (equal). **Mohammad R. Momeni:** Conceptualization (equal); Funding acquisition (equal); Software (supporting); Supervision (equal); Writing – original draft (equal); Writing – review & editing (equal). **Farnaz A. Shakib:** Conceptualization (equal); Funding acquisition (equal); Software (equal); Supervision (equal); Writing – original draft (equal); Writing – review & editing (equal).

DATA AVAILABILITY

The data that support the findings of this study are available from the corresponding authors upon reasonable request. The DL_POLY Quantum software package is available for download at https://github.com/dlpolyquantum/dlpoly_quantum.

APPENDIX A: PIMD FORMALISM IN DIFFERENT COORDINATES

Both staging and normal mode transformations of PIMD are implemented in DL_POLY Quantum and are outlined below in detail.

1. Staging variables

Tuckerman’s “staging variables” method^{53,88} removes the harmonic coupling by introducing a set of staging modes, $\mathbf{q} = \{q_1, \dots, q_n\}$, which are transformed from Cartesian coordinates as

$$\begin{aligned} q_{i,1} &= x_{i,1}, \\ q_{i,k} &= x_{i,k} - \frac{(k-1)x_{i,k+1} + x_{i,1}}{k}, \quad k = 2, \dots, n. \end{aligned} \quad (\text{A1})$$

A staged set of momenta, $\boldsymbol{\pi} = \{p_1, \dots, p_n\}$, are also introduced using the same form of transformation. The PIMD Hamiltonian in the staging variables is

$$\begin{aligned} H_{\text{stage}} = & \sum_{i=1}^N \sum_{k=1}^n \left[\frac{\pi_{i,k}^2}{2m'_{i,k}} + \frac{1}{2} m_{i,k} \omega_n^2 q_{i,k}^2 \right] \\ & + \frac{1}{n} \sum_{k=1}^n V(x_{1,k}(\mathbf{q}), \dots, x_{N,k}(\mathbf{q})), \end{aligned} \quad (\text{A2})$$

where $x_{i,k}(\mathbf{q})$ come from the inverse of the transformation in Eq. (A1) and the masses for each variable are

$$m_{i,1} = 0, \quad m_{i,k} = \frac{k}{k-1} m_i, \quad k = 2, \dots, n. \quad (\text{A3})$$

To increase the efficiency of the method, the fictitious masses are set such that $m'_{i,1} = m_i$ and $m'_{i,k} = m_{i,k}$ for all other values of k .⁸⁸ This ensures that all modes are evolving on the same time scale, removing the problem of the MD time step being limited by the fast modes of the RP oscillations. The transformation to the staging modes is not canonical, resulting in different dynamics than those produced by Eq. (4), but this does not impact the equilibrium statistical quantities.⁸⁸

The EOMs of the staged modes are

$$\begin{aligned} \dot{\pi}_{i,k} &= -m_{i,k} \omega_n^2 q_{i,k} - \frac{1}{n} \sum_{j=1}^n \mathcal{T}_{kj}^{-1\top} \nabla_{x_{ij}} V(\mathbf{x}(\mathbf{Q})), \\ \dot{q}_{i,k} &= \frac{\pi_{i,k}}{m'_{i,k}}, \end{aligned} \quad (\text{A4})$$

where \mathcal{T} is the matrix form of the transformation in Eq. (A1). The integration of the EOMs is done in a straightforward manner using the velocity Verlet algorithm⁸⁹ modified to include the coordinate transformations. For compatibility with existing force calculating algorithms, the positions must be unstaged back into their Cartesian form. The resulting forces are then staged before the momenta are updated, as indicated in the second term in the first momenta derivative in Eq. (A4).

PIMD using staging modes can be performed using three different thermostats: a single NH thermostat,⁵³ a massive NHC thermostat,^{53,55} or the gentle thermostat of Leimkuhler *et al.*⁵⁴ All thermostats are applied to each degree of freedom in the system.

2. Normal modes

The normal modes approach divides the PIMD Hamiltonian into two parts, with their integration treated separately. The first part is the free ring polymer, the first two terms of Eq. (4), and the second is the external potential energy. Transforming the free ring polymer into its normal modes gives a set of n uncoupled harmonic oscillators, which can be evolved exactly.

The transformation into the ring polymer normal modes is done with the matrix,⁵⁶

$$C_{\alpha k} = \begin{cases} \sqrt{1/n}, & k = 0, \\ \sqrt{2/n} \cos(2\pi\alpha k/n), & 1 \leq k \leq n/2 - 1, \\ \sqrt{1/n}(-1)^\alpha, & k = n/2, \\ \sqrt{2/n} \sin(2\pi\alpha k/n), & n/2 + 1 \leq k \leq n - 1, \end{cases} \quad (\text{A5})$$

and the normal mode frequencies are $\omega_k = 2\omega_n \sin(k\pi/n)$. The PIMD Hamiltonian in normal modes is

$$H_{\text{NM}} = \sum_{i=1}^N \sum_{k=0}^{n-1} \left[\frac{\pi_{i,k}^2}{2m_i} + \frac{1}{2} m_i \omega_k^2 q_{i,k}^2 \right] + \frac{1}{n} \sum_{\alpha=1}^n V(x_{1,\alpha}(\mathbf{q}), \dots, x_{N,\alpha}(\mathbf{q})). \quad (\text{A6})$$

A different integration scheme is needed in order to accommodate the separation of the external forces and free ring polymer motion. Similar to the scheme used for the staging modes in Appendix A 1, it is based on the standard velocity Verlet algorithm. In DL_POLY Quantum, it is taken that at the start of each time step, the positions and momenta are in the normal mode coordinates.

First, the forces from the external potential are calculated based on the Cartesian positions. To reduce the overall number of transformations needed to be performed, the forces are then converted into the normal mode basis using

$$\frac{\partial U}{\partial q_{i,k}} = \sum_{\alpha=1}^n C_{\alpha k} \frac{\partial U}{\partial x_{i,\alpha}}. \quad (\text{A7})$$

The normal mode momenta are evolved for half a time step from these forces,

$$\pi_{i,k}\left(t + \frac{\Delta t}{2}\right) = \pi_{i,k}(t) - \frac{\Delta t}{2} \frac{\partial U}{\partial q_{i,k}}. \quad (\text{A8})$$

The free ring polymer evolution of the normal mode positions and momenta is then performed using

$$\begin{pmatrix} \pi_{i,k}(t + \Delta t) \\ q_{i,k}(t + \Delta t) \end{pmatrix} = \begin{pmatrix} \cos(\omega_k \Delta t) & -m_i \omega_k \sin(\omega_k \Delta t) \\ (m_i \omega_k)^{-1} \sin(\omega_k \Delta t) & \cos(\omega_k \Delta t) \end{pmatrix} \times \begin{pmatrix} \pi_{i,k}(t) \\ q_{i,k}(t) \end{pmatrix}. \quad (\text{A9})$$

The centroid ($k = 0$) mode is evolved as $\pi_{i,0}(t + \Delta t) = \pi_{i,0}(t)$ and $q_{i,0}(t + \Delta t) = \frac{\Delta t}{m_i} \pi_{i,0}(t) + q_{i,0}(t)$.

The positions are then transformed back into Cartesian coordinates using

$$x_{i,\alpha} = \sum_{k=0}^{n-1} C_{\alpha k} q_{i,k}. \quad (\text{A10})$$

From there, the forces can be calculated using these new positions, and the normal mode momenta evolved by a second half-a-time step as in Eqs. (A7) and (A8) to complete the propagation of the system a full-time step.

The implementation of the integration scheme in DL_POLY Quantum takes advantage of the efficiencies that arise from connecting multiple time steps together and from transforming the forces from the external potential into the normal mode coordinates. As both the positions and momenta are only evolved in the normal mode coordinates, the only transformation of them from Cartesian coordinates to normal mode coordinates occurs for the initial conditions of the simulation. Similarly, after the initial forces are calculated and transformed, the force transformation only needs to occur once per time step as they carry over to the next time step. The momenta do not need to be transformed back into Cartesian coordinates as part of the propagation. Thus, they are transformed when the Cartesian momenta, or velocities, are needed (e.g., writing trajectory information).

PIMD with normal modes can be performed using several different thermostats. Similar to staging modes, a massive NHC thermostat can be attached to each degree of freedom and is chosen using the keywords **PIMD NM**. In comparison to the staging variables discussed previously, the time step of PIMD in normal modes is by the high-frequency modes, but the canonical nature of the normal mode transformation leads to its use in the real-time PI dynamics methods included in DL_POLY Quantum. Additionally, the PI-specific thermostats, such as PILE and PIGLET, are designed for use with PIMD in normal modes.

APPENDIX B: PIMD SIMULATIONS USING THE PIGLET THERMOSTAT

The PIGLET thermostat can provide a great tool for increasing computational efficiency in large-scale simulations by lowering the number of beads needed to converge the results. This thermostat is rooted in the concept of exploiting the equivalence between non-Markovian dynamics in the generalized Langevin equation (GLE) framework and Markovian dynamics in a higher-dimensional space (p, s) , where n_s auxiliary momenta $s = \{s_i\}$ play a crucial role. These degrees of freedom are subject to linear couplings with both the physical momentum and among themselves. The resulting stochastic differential equation (SDE) can be represented in a concise form,^{57,90}

$$\dot{q} = p, \quad (\text{B1})$$

$$\begin{pmatrix} \dot{p} \\ \dot{s} \end{pmatrix} = \begin{pmatrix} -\nabla V(q) \\ 0 \end{pmatrix} - \begin{pmatrix} a_{pp} & \mathbf{a}^T \\ \bar{a}_p & \mathbf{A} \end{pmatrix} \begin{pmatrix} p \\ s \end{pmatrix} + \begin{pmatrix} b_{pp} & \mathbf{b}^T \\ \bar{b}_p & \mathbf{B} \end{pmatrix} (\xi). \quad (\text{B2})$$

Here, ξ is a vector of $n + 1$ uncorrelated Gaussian random numbers with $\langle \xi_i(t) \xi_j(0) \rangle = \delta_{ij} \delta(t)$. This innovative approach modifies the sampling properties and plays a crucial role in accurately simulating complex quantum systems. By carefully adjusting the parameters associated with the GLE for different normal modes, it is possible to enforce quantum mechanical expectation values, such as $\langle q^2 \rangle$, even when working with a small number of beads.⁸² Additionally, this approach allows us to establish bead-bead correlations that can expedite the convergence of estimators for various other properties of interest.

A simplifying assumption is made in the PIGLET method, assuming $\tilde{T}^{(1)}(\omega) = T$, where T is the target temperature, adhering

to the classical fluctuation-dissipation theorem. Another assumption, $\tilde{T}^{(1)}(\omega) = \tilde{T}(\omega)$, indicates that the same GLE governs all the other ring polymer modes.⁸² This tuned GLE enforces a critical relation, ensuring an accurate representation of quantum expectation values, such as $\langle q^2 \rangle = \hbar/2m\omega \coth(\hbar\omega/2k_B T)$. In essence, this approach ensures that quantum expectation values are accurately represented, even when working with a lower number of beads, and that bead-bead correlations are consistent with the desired quantum behavior of the system.⁹¹

The successful implementation of PIGLET within the PIMD framework hinges on obtaining and utilizing specialized matrices known as the A-Matrix (drift matrix) and C-Matrix (diffusion matrix). These matrices are pivotal in configuring the PIGLET thermostat and ensuring its effective operation. The A-Matrix represents the drift term in the equations of motion that govern the system's dynamics under the influence of the PIGLET thermostat. It encapsulates the deterministic forces acting on the particles and is essential for accurately modeling the system's behavior. The A-Matrix helps dictate the trajectories and positions of the particles as they evolve over time. The C-Matrix, on the other hand, accounts for the stochastic forces introduced by the thermostat. These stochastic forces are a key element of the Langevin-like dynamics that the PIGLET thermostat imparts to the system. The C-Matrix captures the fluctuating components of the forces, representing the thermal noise that influences the system's motion. To be implemented in DL_POLY Quantum 2.0, these parametric matrices are obtained from the GLE4MD website (<https://gle4md.org>).⁹²

APPENDIX C: DERIVATION OF BTW-LJ FF

The BTW-FF has the parameterization of the functional form of the MM3⁹³ force field,

$$\begin{aligned} E_{total} &= E_{bonded} + E_{nonbonded}, \\ E_{bonded} &= \sum E_{bond} + \sum E_{angle} + \sum E_{torsion}, \\ E_{nonbonded} &= \sum (E_{vdW} + E_{Coul}). \end{aligned} \quad (\text{C1})$$

The bond and angle terms of the bonded interactions are modeled as higher-order polynomial functions, while dihedral and improper terms are modeled as the usual Fourier series terms. The non-bonded energy term includes van der Waals (vdW) interactions in the form of Buckingham potential and Coulomb forces. The Buckingham potential is defined as

$$E_{Buck} = \varepsilon_0 \left[A \exp\left(-B \frac{r}{r_0}\right) - C \left(\frac{r_0}{r}\right)^6 \right], \quad (\text{C2})$$

where r_0 is the distance at minimum potential and ε_0 is the depth of the potential well, with default values for A, B, and C constants used are 184 000, 12, and 2.25, respectively. Unlike Lennard-Jones (LJ) potential,

$$E_{LJ} = 4\varepsilon \left[\left(\frac{\sigma}{r}\right)^{12} - \left(\frac{\sigma}{r}\right)^6 \right], \quad (\text{C3})$$

Buckingham (Buck) potential has an exponential repulsive part that can reach a maximum at very short distances and falls off negative infinity (see Fig. 7). This artifact causes problems for soft

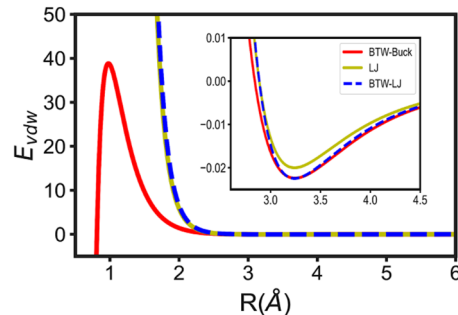


FIG. 7. Comparison of vdW interaction potentials in Buckingham and Lennard-Jones forms. The inset compares the depth of normal LJ, modified LJ in BTW-LJ FF, and Buckingham potential in BTW FF.

vdW potentials and high temperature, and numerical instabilities can arise.⁷⁷ To avoid this numerical instability of simulation, we have converted Buckingham parameters into LJ-type parameters as follows:

$$\sigma = \frac{r_0}{2^{1/6}}, \quad \varepsilon = 2^{1/6} \varepsilon_0. \quad (\text{C4})$$

This modification reproduces strong repulsive force at a short distance with correct potential depth as of the Buckingham potential, as seen in the inset of Fig. 7.

We derived parameters in Eq. (C4) by rewriting Buckingham potential as Exponential-6 function at a loose form⁹⁴ of

$$E_{Buck} = \varepsilon \left[\frac{\beta}{\alpha - \beta} \exp\left\{\alpha\left(1 - \frac{r}{r_0}\right)\right\} - \frac{\alpha}{\alpha - \beta} \left(\frac{r_0}{r}\right)^\beta \right] \quad (\text{C5})$$

with $\alpha = 12$, and $\beta = 6$ gives

$$E_{Buck} = \varepsilon \left[\exp(12) \exp\left(-12 \frac{r}{r_0}\right) - 2 \left(\frac{r_0}{r}\right)^6 \right]. \quad (\text{C6})$$

By comparing Eqs. (C2) and (C6), we obtain

$$\varepsilon = \frac{A}{\exp(12)} \varepsilon_0 \approx \sqrt[6]{2} \varepsilon_0, \quad \text{OR,} \quad \varepsilon = \frac{C}{2} \varepsilon_0 \approx \sqrt[6]{2} \varepsilon_0. \quad (\text{C7})$$

Alternatively, we obtain the Buckingham to LJ type parameters by the imposition of an equal energy integral from the potential well depth's minimum to infinite interatomic distance,⁹⁴

$$\int_{r_0}^{\infty} E_{Buck} dr = \int_{r_0}^{\infty} E_{LJ} dr, \quad (\text{C8})$$

and this gives

$$\begin{aligned} \varepsilon_0 \left[-A \frac{\exp\left(-\frac{B}{r_0} r\right)}{\frac{B}{r_0}} + C \frac{r_0^6}{5r^5} \right]_{r_0}^{\infty} &= 4\varepsilon \left[-\frac{\sigma^{12}}{11r^{11}} + \frac{\sigma^6}{5r^5} \right]_{r_0}^{\infty} \\ - \varepsilon_0 \left[C \frac{r_0^6}{5r_0^5} - A \frac{\exp\left(-\frac{B}{r_0} r_0\right)}{\frac{B}{r_0}} \right] &= -4\varepsilon \left[\frac{\sigma^6}{5r_0^5} - \frac{\sigma^{12}}{11r_0^{11}} \right]; \end{aligned} \quad (\text{C9})$$

replacing with $r_o = \sqrt[6]{2} \sigma$, we get

$$\varepsilon = \frac{55\varepsilon_0}{17} \left(\frac{C}{5} - A \frac{\exp(-B)}{B} \right). \quad (\text{C10})$$

For the given A, B, and C values of 184000, 12, and 2.25, respectively, we obtain $\varepsilon = 1.151 \varepsilon_0 \approx \sqrt[6]{2} \varepsilon_0$. The BTW-LJ force field for HKUST-1 is implemented in DL_POLY Quantum 2.0, introduced here.

REFERENCES

- ¹B. J. Alder and T. E. Wainwright, "Studies in molecular dynamics. I. General method," *J. Chem. Phys.* **31**, 459–466 (1959).
- ²D. Chandler, "From 50 years ago, the birth of modern liquid-state science," *Annu. Rev. Phys. Chem.* **68**, 19–38 (2017).
- ³M. P. Allen and D. J. Tildesley, *Computer Simulation of Liquids*, 2nd ed. (Oxford University Press, 2017).
- ⁴M. E. Tuckerman, *Statistical Mechanics: Theory and Molecular Simulation*, 2nd ed. (Oxford University Press, 2023).
- ⁵A. Rimola, D. Costa, M. Sodupe, J.-F. Lambert, and P. Ugliengo, "Silica surface features and their role in the adsorption of biomolecules: Computational modeling and experiments," *Chem. Rev.* **113**, 4216–4313 (2013).
- ⁶P. Li and K. M. Merz, Jr., "Metal ion modeling using classical mechanics," *Chem. Rev.* **117**, 1564–1686 (2017).
- ⁷B. B. Hansen, S. Spittle, B. Chen, D. Poe, Y. Zhang, J. M. Klein, A. Horton, L. Adhikari, T. Zelovich, B. W. Doherty, B. Gurkan, E. J. Maginn, A. Ragauskas, M. Dadmun, T. A. Zawodzinski, G. A. Baker, M. E. Tuckerman, R. F. Savinell, and J. R. Sangoro, "Deep eutectic solvents: A review of fundamentals and applications," *Chem. Rev.* **121**, 1232–1285 (2021).
- ⁸A. Vidal-Limon, J. E. Aguilar-Toala, and A. M. Liceaga, "Integration of molecular docking analysis and molecular dynamics simulations for studying food proteins and bioactive peptides," *J. Agric. Food Chem.* **70**, 934–943 (2022).
- ⁹M. Born and R. Oppenheimer, "Zur quantentheorie der moleküle," *Ann. Phys.* **389**, 457–484 (1927).
- ¹⁰T. Markland and M. Ceriotti, "Nuclear quantum effects enter the mainstream," *Nat. Rev. Chem.* **2**, 0109 (2018).
- ¹¹L. D. Fosdick, "Numerical estimation of the partition function in quantum statistics," *J. Math. Phys.* **3**, 1251–1264 (1962).
- ¹²L. D. Fosdick and H. F. Jordan, "Path-integral calculation of the two-particle slater sum for He⁴," *Phys. Rev.* **143**, 58–66 (1966).
- ¹³J. A. Barker, "A quantum-statistical Monte Carlo method; path integrals with boundary conditions," *J. Chem. Phys.* **70**, 2914–2918 (1979).
- ¹⁴D. Chandler and P. G. Wolynes, "Exploiting the isomorphism between quantum theory and classical statistical mechanics of polyatomic fluids," *J. Chem. Phys.* **74**, 4078–4095 (1981).
- ¹⁵R. P. Feynman and A. R. Hibbs, *Quantum Mechanics and Path Integrals*, Emended ed. (Dover Publications, 2005).
- ¹⁶G. A. Voth, "Path-integral centroid methods in quantum statistical mechanics and dynamics," in *Advances in Chemical Physics* (John Wiley & Sons Ltd, 1996), pp. 135–218.
- ¹⁷S. Habershon, D. E. Manolopoulos, T. E. Markland, and T. F. Miller, "Ring-polymer molecular dynamics: Quantum effects in chemical dynamics from Classical Trajectories in an extended phase space," *Annu. Rev. Phys. Chem.* **64**, 387–413 (2013).
- ¹⁸B. Hirshberg, V. Rizzi, and M. Parrinello, "Path integral molecular dynamics for bosons," *Proc. Natl. Acad. Sci. U. S. A.* **116**, 21445–21449 (2019).
- ¹⁹M. Parrinello and A. Rahman, "Study of an F center in molten kcl," *J. Chem. Phys.* **80**, 860–867 (1984).
- ²⁰J. Cao and G. A. Voth, "The formulation of quantum statistical mechanics based on the Feynman path centroid density. IV. Algorithms for centroid molecular dynamics," *J. Chem. Phys.* **101**, 6168–6183 (1994).
- ²¹S. Jang and G. A. Voth, "Path integral centroid variables and the formulation of their exact real time dynamics," *J. Chem. Phys.* **111**, 2357–2370 (1999).
- ²²S. Jang and G. A. Voth, "A derivation of centroid molecular dynamics and other approximate time evolution methods for path integral centroid variables," *J. Chem. Phys.* **111**, 2371–2384 (1999).
- ²³I. R. Craig and D. E. Manolopoulos, "Quantum statistics and classical mechanics: Real time correlation functions from ring polymer molecular dynamics," *J. Chem. Phys.* **121**, 3368–3373 (2004).
- ²⁴I. R. Craig and D. E. Manolopoulos, "Chemical reaction rates from ring polymer molecular dynamics," *J. Chem. Phys.* **122**, 084106 (2005).
- ²⁵I. R. Craig and D. E. Manolopoulos, "A refined ring polymer molecular dynamics theory of chemical reaction rates," *J. Chem. Phys.* **123**, 034102 (2005).
- ²⁶P. Shushkov, R. Li, and J. C. Tully, "Ring polymer molecular dynamics with surface hopping," *J. Chem. Phys.* **137**, 22A549 (2012).
- ²⁷J. O. Richardson and M. Thoss, "Communication: Nonadiabatic ring-polymer molecular dynamics," *J. Chem. Phys.* **139**, 031102 (2013).
- ²⁸N. Ananth, "Mapping variable ring polymer molecular dynamics: A path-integral based method for nonadiabatic processes," *J. Chem. Phys.* **139**, 124102 (2013).
- ²⁹S. N. Chowdhury and P. Huo, "Coherent state mapping ring polymer molecular dynamics for non-adiabatic quantum propagations," *J. Chem. Phys.* **147**, 214109 (2017).
- ³⁰F. A. Shakib and P. Huo, "Ring polymer surface hopping: Incorporating nuclear quantum effects into nonadiabatic molecular dynamics simulations," *J. Phys. Chem. Lett.* **8**, 3073–3080 (2017).
- ³¹D. K. Limbu and F. A. Shakib, "Real-time dynamics and detailed balance in ring polymer surface hopping: The impact of frustrated hops," *J. Phys. Chem. Lett.* **14**, 8658–8666 (2023).
- ³²D. K. Limbu and F. A. Shakib, "SHARP pack: A modular software for incorporating nuclear quantum effects into non-adiabatic dynamics simulations," *Software Impacts* **19**, 100604 (2024).
- ³³S. Habershon, G. S. Fanourgakis, and D. E. Manolopoulos, "Comparison of path integral molecular dynamics methods for the infrared absorption spectrum of liquid water," *J. Chem. Phys.* **129**, 074501 (2008).
- ³⁴A. Witt, S. D. Ivanov, M. Shiga, H. Forbert, and D. Marx, "On the applicability of centroid and ring polymer path integral molecular dynamics for vibrational spectroscopy," *J. Chem. Phys.* **130**, 194510 (2009).
- ³⁵V. Kapil, M. Rossi, O. Marsalek, R. Petraglia, Y. Litman, T. Spura, B. Cheng, A. Cuzzocrea, R. H. Meißner, D. M. Wilkins, B. A. Helfrecht, P. Juda, S. P. Bienvenue, W. Fang, J. Kessler, I. Poltavsky, S. Vandenbrande, J. Wieme, C. Corminboeuf, T. D. Kühne, D. E. Manolopoulos, T. E. Markland, J. O. Richardson, A. Tkatchenko, G. A. Tribello, V. Van Speybroeck, and M. Ceriotti, "I-PI 2.0: A universal force engine for advanced molecular simulations," *Comput. Phys. Commun.* **236**, 214–223 (2019).
- ³⁶T. E. Markland and D. E. Manolopoulos, "An efficient ring polymer contraction scheme for imaginary time path integral simulations," *J. Chem. Phys.* **129**, 024105 (2008).
- ³⁷V. Kapil, J. VandeVondele, and M. Ceriotti, "Accurate molecular dynamics and nuclear quantum effects at low cost by multiple steps in real and imaginary time: Using density functional theory to accelerate wavefunction methods," *J. Chem. Phys.* **144**, 054111 (2016).
- ³⁸M. Tuckerman, B. J. Berne, and G. J. Martyna, "Reversible multiple time scale molecular dynamics," *J. Chem. Phys.* **97**, 1990–2001 (1992).
- ³⁹A. P. Thompson, H. M. Aktulgä, R. Berger, D. S. Bolintineanu, W. M. Brown, P. S. Crozier, P. J. in 't Veld, A. Kohlmeyer, S. G. Moore, T. D. Nguyen, R. Shan, M. J. Stevens, J. Tranchida, C. Trott, and S. J. Plimpton, "LAMMPS—A flexible simulation tool for particle-based materials modeling at the atomic, meso, and continuum scales," *Comput. Phys. Commun.* **271**, 108171 (2022).
- ⁴⁰M. R. Momeni and F. A. Shakib, "DL_POLY Quantum molecular simulation package," available from https://github.com/fashakib/DL_POLY-Quantum-v1.0.
- ⁴¹W. Smith, T. R. Forester, and I. T. Todorov, "DL_POLY Classic molecular simulation package," STFC Daresbury Laboratory, available from https://gitlab.com/DL_POLY_Classic.
- ⁴²R. P. Feynman, A. R. Hibbs, and D. F. Styer, "Quantum mechanics and path integrals," Courier Corporation, 2010.
- ⁴³H. F. Trotter, "On the product of semi-groups of operators," *Proc. Am. Math. Soc.* **10**, 545–551 (1959).

- ⁴⁴R. Colleopardo-Guevara, I. R. Craig, and D. E. Manolopoulos, "Proton transfer in a polar solvent from ring polymer reaction rate theory," *J. Chem. Phys.* **128**, 144502 (2008).
- ⁴⁵R. L. Kenion and N. Ananth, "Direct simulation of electron transfer in the cobalt hexammine(II/III) self-exchange reaction," *Phys. Chem. Chem. Phys.* **18**, 26117–26124 (2016).
- ⁴⁶J. S. Kretchmer and T. F. I. Miller, "Tipping the balance between concerted versus sequential proton-coupled electron transfer," *Inorg. Chem.* **55**, 1022–1031 (2016).
- ⁴⁷T. D. Hone, P. J. Rossky, and G. A. Voth, "A comparative study of imaginary time path integral based methods for quantum dynamics," *J. Chem. Phys.* **124**, 154103 (2006).
- ⁴⁸S. Habershon, T. E. Markland, and D. E. Manolopoulos, "Competing quantum effects in the dynamics of a flexible water model," *J. Chem. Phys.* **131**, 024501 (2009).
- ⁴⁹M. Suzuki, "General theory of fractal path integrals with applications to many-body theories and statistical physics," *J. Math. Phys.* **32**, 400–407 (1991).
- ⁵⁰H. Yoshida, "Construction of higher order symplectic integrators," *Phys. Lett. A* **150**, 262–268 (1990).
- ⁵¹G. J. Martyna, M. E. Tuckerman, and M. L. Klein, "Explicit reversible integrators for extended systems dynamics," *Mol. Phys.* **87**, 1117–1157 (1996).
- ⁵²G. J. Martyna, D. J. Tobias, and M. L. Klein, "Constant pressure molecular dynamics algorithms," *J. Chem. Phys.* **101**, 4177–4189 (1994).
- ⁵³M. E. Tuckerman, B. J. Berne, G. J. Martyna, and M. L. Klein, "Efficient molecular dynamics and hybrid Monte Carlo algorithms for path integrals," *J. Chem. Phys.* **99**, 2796–2808 (1993).
- ⁵⁴B. Leimkuhler, E. Noorizadeh, and F. Theil, "A gentle stochastic thermostat for molecular dynamics," *J. Stat. Phys.* **135**, 261–277 (2009).
- ⁵⁵G. J. Martyna, M. L. Klein, and M. Tuckerman, "Nosé-Hoover chains: The canonical ensemble via continuous dynamics," *J. Chem. Phys.* **97**, 2635–2643 (1992).
- ⁵⁶M. Ceriotti, M. Parrinello, T. E. Markland, and D. E. Manolopoulos, "Efficient stochastic thermostating of path integral molecular dynamics," *J. Chem. Phys.* **133**, 124104 (2010).
- ⁵⁷M. Ceriotti, D. E. Manolopoulos, and M. Parrinello, "Accelerating the convergence of path integral dynamics with a generalized Langevin equation," *J. Chem. Phys.* **134**, 084104 (2011).
- ⁵⁸M. Rossi, M. Ceriotti, and D. E. Manolopoulos, "How to remove the spurious resonances from ring polymer molecular dynamics," *J. Chem. Phys.* **140**, 234116 (2014).
- ⁵⁹W. Smith, "Molecular dynamics on hypercube parallel computers," *Comput. Phys. Commun.* **62**, 229–248 (1991).
- ⁶⁰W. Smith, "Molecular dynamics on distributed memory (MIMD) parallel computers," *Theor. Chim. Acta* **84**, 385–398 (1993).
- ⁶¹W. Xia, A. Mahmood, R. Zou, and Q. Xu, "Metal–organic frameworks and their derived nanostructures for electrochemical energy storage and conversion," *Energy Environ. Sci.* **8**, 1837–1866 (2015).
- ⁶²A. E. Baumann, D. A. Burns, B. Liu, and V. S. Thoi, "Metal–organic framework functionalization and design strategies for advanced electrochemical energy storage devices," *Commun. Chem.* **2**, 86 (2019).
- ⁶³T. Qiu, Z. Liang, W. Guo, H. Tabassum, S. Gao, and R. Zou, "Metal–organic framework-based materials for energy conversion and storage," *ACS Energy Lett.* **5**, 520–532 (2020).
- ⁶⁴D. Farrusseng, S. Aguado, and C. Pinel, "Metal–organic frameworks: Opportunities for catalysis," *Angew. Chem., Int. Ed.* **48**, 7502–7513 (2009).
- ⁶⁵L. Zhu, X.-Q. Liu, H.-L. Jiang, and L.-B. Sun, "Metal–organic frameworks for heterogeneous basic catalysis," *Chem. Rev.* **117**, 8129–8176 (2017).
- ⁶⁶V. Bernales, M. A. Ortuño, D. G. Truhlar, C. J. Cramer, and L. Gagliardi, "Computational design of functionalized metal–organic framework nodes for catalysis," *ACS Cent. Sci.* **4**, 5–19 (2018).
- ⁶⁷M. R. Momeni and F. A. Shakib, "Deterministic role of structural flexibility on catalytic activity of conductive 2D layered metal–organic frameworks," *Chem. Commun.* **57**, 315–318 (2021).
- ⁶⁸Z. Meng, R. M. Stoltz, L. Mendecki, and K. A. Mirica, "Electrically-transduced chemical sensors based on two-dimensional nanomaterials," *Chem. Rev.* **119**, 478–598 (2019).
- ⁶⁹L. S. Xie, G. Skorupskii, and M. Dincă, "Electrically conductive metal–organic frameworks," *Chem. Rev.* **120**, 8536–8580 (2020).
- ⁷⁰M. R. Momeni, Z. Zhang, D. Dell'Angelo, and F. A. Shakib, "Tuning electronic properties of conductive 2D layered metal–organic frameworks via host–guest interactions: Dioxygen as an electroactive chemical stimuli," *APL Mater.* **9**, 051109 (2021).
- ⁷¹Z. Zhang, D. Dell'Angelo, M. R. Momeni, Y. Shi, and F. A. Shakib, "Metal-to-semiconductor transition in two-dimensional metal–organic frameworks: An ab initio dynamics perspective," *ACS Appl. Mater. Interfaces* **13**, 25270–25279 (2021).
- ⁷²Z. Zhang, D. S. Valente, Y. Shi, D. K. Limbu, M. R. Momeni, and F. A. Shakib, "In silico high-throughput design and prediction of structural and electronic properties of low-dimensional metal–organic frameworks," *ACS Appl. Mater. Interfaces* **15**, 9494–9507 (2023).
- ⁷³H. Kim, S. Yang, S. R. Rao, S. Narayanan, E. A. Kapustin, H. Furukawa, A. S. Umans, O. M. Yaghi, and E. N. Wang, "Water harvesting from air with metal–organic frameworks powered by natural sunlight," *Science* **356**, 430–434 (2017).
- ⁷⁴W. Xu and O. M. Yaghi, "Metal–organic frameworks for water harvesting from air, anywhere, anytime," *ACS Cent. Sci.* **6**, 1348–1354 (2020).
- ⁷⁵W. Song, Z. Zheng, A. H. Alawadhi, and O. M. Yaghi, "Mof water harvester produces water from death valley desert air in ambient sunlight," *Nat. Water* **1**, 626–634 (2023).
- ⁷⁶M. A. Addicoat, N. Vankova, I. F. Akter, and T. Heine, "Extension of the universal force field to metal–organic frameworks," *J. Chem. Theory Comput.* **10**, 880–891 (2014).
- ⁷⁷S. Bureekaew, S. Amirjalayer, M. Tafipolsky, C. Spickermann, T. K. Roy, and R. Schmid, "MOF-FF—A flexible first-principles derived force field for metal–organic frameworks," *Phys. Status Solidi B* **250**, 1128–1141 (2013).
- ⁷⁸J. K. Bristow, D. Tiana, and A. Walsh, "Transferable force field for metal–organic frameworks from first-principles: BTW-FF," *J. Chem. Theory Comput.* **10**, 4644–4652 (2014).
- ⁷⁹A. J. Rieth, K. M. Hunter, M. Dincă, and F. Paesani, "Hydrogen bonding structure of confined water templated by a metal–organic framework with open metal sites," *Nat. Commun.* **10**, 4771 (2019).
- ⁸⁰Y. Shi, M. R. Momeni, Y.-J. Chen, D. K. Limbu, Z. Zhang, and F. A. Shakib, "Water induced structural transformations in flexible two-dimensional layered conductive metal–organic frameworks," *Chem. Mater.* **34**, 7730–7740 (2022).
- ⁸¹Y. Wu, A. Kobayashi, G. J. Halder, V. K. Peterson, K. W. Chapman, N. Lock, P. D. Southon, and C. J. Kepert, "Negative thermal expansion in the metal–organic framework material Cu₃(1,3,5-benzenetricarboxylate)₂," *Angew. Chem., Int. Ed.* **47**, 8929–8932 (2008).
- ⁸²M. Ceriotti and D. E. Manolopoulos, "Efficient first-principles calculation of the quantum kinetic energy and momentum distribution of nuclei," *Phys. Rev. Lett.* **109**, 100604 (2012).
- ⁸³J. E. Bertie and Z. Lan, "Infrared intensities of liquids XX: The intensity of the OH stretching band of liquid water revisited, and the best current values of the optical constants of H₂O(l) at 25°C between 15,000 and 1 cm⁻¹," *Appl. Spectrosc.* **50**, 1047–1057 (1996).
- ⁸⁴A. E. I. DePrince and J. R. Hammond, "Coupled cluster theory on graphics processing units I. The coupled cluster doubles method," *J. Chem. Theory Comput.* **7**, 1287–1295 (2011).
- ⁸⁵I. S. Ufimtsev and T. J. Martínez, "Graphical processing units for quantum chemistry," *Comput. Sci. Eng.* **10**, 26–34 (2008).
- ⁸⁶I. S. Ufimtsev and T. J. Martínez, "Quantum chemistry on graphical processing units. 3. Analytical energy gradients, geometry optimization, and first principles molecular dynamics," *J. Chem. Theory Comput.* **5**, 2619–2628 (2009).
- ⁸⁷T. J. Boerner, S. Deems, T. R. Furlani, S. L. Knuth, and J. Towns, "Access: Advancing innovation: NSF's advanced cyberinfrastructure coordination ecosystem: Services & support," in *Practice and Experience in Advanced Research Computing, PEARC'23* (Association for Computing Machinery, New York, 2023), pp. 173–176.

- ⁸⁸A. Pérez, M. E. Tuckerman, and M. H. Müser, “A comparative study of the centroid and ring-polymer molecular dynamics methods for approximating quantum time correlation functions from path integrals,” *J. Chem. Phys.* **130**, 184105 (2009).
- ⁸⁹L. Verlet, “Computer experiments’ on classical fluids. I. Thermodynamical properties of Lennard-Jones molecules,” *Phys. Rev.* **159**, 98–103 (1967).
- ⁹⁰M. Ceriotti, G. Bussi, and M. Parrinello, “Colored-noise thermostats à la carte,” *J. Chem. Theory Comput.* **6**, 1170–1180 (2010).
- ⁹¹F. Uhl, D. Marx, and M. Ceriotti, “Accelerated path integral methods for atomistic simulations at ultra-low temperatures,” *J. Chem. Phys.* **145**, 054101 (2016).
- ⁹²M. Ceriotti, <https://epfl-cosmo.github.io/gle4md/>, 2016.
- ⁹³N. L. Allinger, Y. H. Yuh, and J. H. Lii, “Molecular mechanics. The MM3 force field for hydrocarbons. I,” *J. Am. Chem. Soc.* **111**, 8551–8566 (1989).
- ⁹⁴T.-C. Lim, “Alignment of buckingham parameters to generalized Lennard-Jones potential functions,” *Z. Naturforsch. A* **64**, 200–204 (2009).